PROCEEDINGS OF SPIE

Power-efficient lumped-element meandered silicon Mach-Zehnder modulators

Sharif Azadeh, S., Nojić, J., Moscoso-Mártir, A., Merget, F., Witzens, J.

SPIE.

Event: SPIE OPTO, 2020, San Francisco, California, United States

Power-efficient lumped-element meandered silicon Mach-Zehnder modulators

S. Sharif Azadeh[1,2], J. Nojić[1], A. Moscoso-Mártir[1], F. Merget[1], J. Witzens*[1]

[1] Institute for Integrated Photonics, RWTH Aachen University,
Campus Blvd. 73, 52074 Aachen, Germany
[2] Now at NINT department, Max Planck Institute for Microstructure Physics, Weinberg 2, Halle, Germany

ABSTRACT

Driving electro-optic modulators in lumped-element (LE) configuration allows for small footprint, reduced power consumption, and improved high-speed performance. The main shortcoming of conventional rectilinear LE modulators are the required high drive-voltages, resulting from their shortened phase-shifters. To address this, we introduce a Mach-Zehnder modulator with meandered phase shifters (M-MZM), which can be driven in LE configuration, while keeping the optical phase shifter length in the same order as traveling-wave modulators (TW-MZMs). A design limitation that needs to be taken into account consists in the optical transit time of the device, that limits the overall electro-optic bandwidth. First, we review the overall power consumption improvement as well as the bandwidth enhancement in LE modulators compared to TW-MZMs, also taking the driver output impedance and parasitics from wire- or bump-bonds into account. Then, we report on the design, implementation, and experimental characterization of carrier-depletion based M-MZMs fabricated on silicon-on-insulator (SOI) wafers using standard CMOS-compatible processes. The fabricated M-MZMs, provided with low (W1), moderately (W2) and highly (W3) doped junctions, require 9.2 V_{pp}, 5.5 V_{pp}, and 3.7 V_{pp} for full extinction, with optical insertion losses of 5 dB, 6.3 dB and 9.1 dB. For all three M-MZMs, open eye diagrams are recorded at 25 Gb/s using a 50 Ω driver and termination. For unterminated M-MZMs, higher data rates could be achieved, provided that a low output impedance driver be wire- or bump-bonded to the modulators. Finally, we compare the power consumption of the M-MZMs with TW-MZMs and show that the M-MZMs feature a 4X reduced power consumption at 25 Gb/s.

Keywords: Optical Interconnects, Silicon Photonics, Electro-Optic Modulators.

1. INTRODUCTION

Silicon photonics (SiP) electro-optic modulators have reached a high level of maturity both in terms of modulation speed and optical loss [1,2], allowing them the meet the requirements of 400G transceiver systems [3,4]. Their compatibility with accessible CMOS fabrication infrastructure makes them a cost-effective solution for mass-produced single mode fiber output transceivers [5]. Nevertheless, with the growing global internet traffic expected to triple until the year 2022 and to reach 350 Exabytes per month [6], reducing the power consumption of optical transceivers and of electro-optic modulators in particular (in terms of J/bit) remains a requirement.

In an electro-optic modulator, the main sources of power consumption can be classified into three categories: 1. radio frequency (RF) power consumption (required to actuate the optical output), 2. DC power consumption (e.g. thermal phase shifters used to bias the modulator or DC current through termination resistors at bias point), and 3. power consumption of an active control system required to bias the modulators. A power-efficient modulator should reduce the power consumption taking all three sources into account.

Due to the absence of an efficient electro-optic effect in bulk silicon [7], the majority of all-silicon modulators utilize the free carrier plasma-dispersion effect as the modulation mechanism, typically realized in a reverse biased pn junction for high speed operation [8]. Two main configurations have been extensively used to employ this effect in silicon modulators, both offering high data rates and acceptable insertion losses [8,9]: 1) Travelling wave Mach-Zehnder modulators (TW-MZMs), and 2) ring resonator modulators (RRMs). The RF power consumption of RRMs (and more generally resonance based modulators) can be orders of magnitude lower than TW-MZMs, as it is reduced by a factor scaling with the finesse (F) of the resonance. Moreover, as other forms of lumped-element (LE) modulators, they do not require a termination

*jwitzens@iph.rwth-aachen.de; phone +49 241 80 20020; www.iph.rwth-aachen.de

resistor, further reducing their power consumption relative to TW-based devices [9]. However, RRMs typically necessitate active stabilization of their resonance frequency due to their limited optical bandwidth (<0.2 nm). In contrast, TW-MZMs, despite having a higher RF power consumption, are much easier to bias, thanks to their high optical bandwidth. To mitigate these limitations of resonantly enhanced devices, many efforts have been made in recent years to develop novel modulator configurations such as ring assisted Mach-Zehnder modulators (RA-MZMs) with spoiled quality factors [10] as well as slow light photonic crystal (PC) MZM configurations [11], aiming at resonant or slow light enhancement while keeping the optical bandwidth at a moderately high level (3-5 nm) to remove the need for or facilitate active control. Unlike TW-MZMs, such devices have relatively small phase shifter lengths and behave as LE phase shifters, which allows for operation without an RF termination, and thus further reduction of the power consumption. In particular, in [12], using a RA-MZM structure, a stable modulation performance was achieved over a 60 degree temperature range, while a $V_\pi l$ resonance enhancement by a factor 7 (at the resonance frequency) allowed for a moderately low drive voltage despite the short length of the device. However, RA-MZMs and PC modulators have not become the mainstream solution, mainly because they both are more sensitive to fabrication inaccuracies, as compared to rectilinear phase shifters. Taking variability of laser emission wavelengths and resonance frequencies resulting from fabrication tolerances into account, these operation ranges remain borderline to enable operation in a data center environment without any temperature stabilization or other resonance tuning mechanism. Here, we pursue a simpler approach based on an MZM with meandered phase shifters in each arm. While this does not provide resonance enhancement, the meandered Mach-Zehnder modulator (M-MZM) has a smaller RF power consumption relative to TW-MZMs owing to the phase shifters behaving as lumped-elements (Section 2). Lumped-element performance is obtained for relatively long optical phase shifter lengths by decoupling the optical length from the RF length, as explained in Section 3. In contrast to resonance based modulators such as RRMs, M-MZMs have a higher RF power consumption. However, their optically wideband range of operation allows them to perform with much reduced control system requirements. The total optical length of the phase shifters is primarily limited by the transit time of the light, that limits the electro-optic cutoff frequency of the device.

2. PERFORMANCE METRICS OF LUMPED ELEMENT MODULATORS

Prior to discussing the specificities of the M-MZM, we briefly review how bandwidth and power consumption of LE modulators compares to that of TW-MZMs. Lumped element configuration refers to a device which is sufficiently small relative to the RF wavelength in the device ($\lambda_{RF} = \lambda_0/n_{RF}$, with λ_0 the free space RF wavelength and n_{RF} the RF index) for it to be considered a point load from an RF point of view. An often used criterion is for a device to be shorter than one tenth of the RF wavelength. However, the boundary is not abrupt and lengthening the device rather gradually penalizes the bandwidth.

Although TW-MZMs require lower drive voltages due to their long phase shifters and are generally optically wideband, they suffer from higher power consumption, as the RF signal is terminated at the end of the transmission line. Moreover, the main factor limiting the bandwidth in travelling wave modulators is the RF loss along the transmission line. In a LE modulator, both termination and RF attenuation along the device are absent, so that the LE modulators potentially allow for fast and power-efficient modulation. However, the short phase shifter length in conventional LE modulators penalizes the achieved phase shift and thus results in a need for high drive voltages. This increases again the power consumption, since the required energy per bit in a LE modulator is expressed as [13]

$$E_{bit} = \frac{1}{4} C V_D^2 \qquad (1)$$

and quadratically increases with the drive-voltage V_D. In this equation, C refers to the total capacitance of the device and scales with the length of the phase shifters. Thus, one might suggest that by increasing the phase shifter length, power consumption can be reduced, since doubling the length (l) results in a two times higher capacitance C, but also reduces the required drive voltage V_D to half, and thus E_{bit} is reduced by a factor 2 (ignoring nonlinearities of the device capacitance and of the charge dependent phase shift). In a conventional rectilinear lumped element modulator, the length of the phase shifter is however constrained by the LE condition. Distributed drivers provide a way to drive series of LE phase shifter elements without being limited by phase matching and the ensuing limitation on cumulative phase shifter length [14]. They do however require monolithic integration of electronics or more complex packaging schemes such as bump-bonding. We rather propose to decouple the optical phase shifter length from the RF length of the device, using a meandered MZM as presented in Section 3. The device is designed in a way to be short from an RF point of view and to remain a point load

up several tens of gigahertz, but to have a looped optically long phase shifter (1.4 mm) of comparable length to that of travelling wave modulators.

2.1 Bandwidth limitations in LE modulators

Generally, there are two factors limiting the bandwidth of a LE modulator: 1) The RF signal transferred to the device at high speeds, i.e., the speed at which the phase shifter can be actuated in the electrical domain [see Fig. 1(a)], and 2) the time taken by light to transit through the phase shifter. We describe the two limiting factors independently.

Electrical cutoff frequency

The actuation speed is typically limited primarily by the capacitance and series impedance. Here, it is useful to define the intrinsic cutoff frequency of the phase shifter (f_{RC}), that is, the maximum cutoff frequency the modulator can reach irrespectively of external circuitry. In the absence of signal pre-emphasis, it can be expressed as [9]

$$f_{RC} = \frac{1}{2\pi RC} = \frac{1}{2\pi(R_l/l)(C_l \cdot l)} = \frac{1}{2\pi R_l C_l} \tag{2}$$

with R and C being respectively the total series resistance and total capacitance of the device, R_l and C_l the linear resistance ($\Omega \cdot m$) and capacitance (F/m), and l the total device length. The intrinsic bandwidth is independent of the device length, since R and C scale with $1/l$ and l, respectively. In practice, however, as shown in Fig. 1(a), the output impedance of the driver (or a 50 Ω cable connecting the device to the RF source) reduces the cutoff frequency, as the time constant increases to $(R_l + l \cdot R_{dr})C_l$, and the aggregate bandwidth can be written as [9]

$$f_{-3dB,RC} = \frac{1}{2\pi(R_l/l + R_{dr})(C_l \cdot l)} = \frac{1}{2\pi(R_l C_l + R_{dr} C_l l)} \tag{3}$$

The actual bandwidth of LE modulators thus depends both on the device length and on the output impedance of the driver. It is thus beneficial to use low output impedance drivers for LE modulators, to get closer to the intrinsic cutoff frequency.
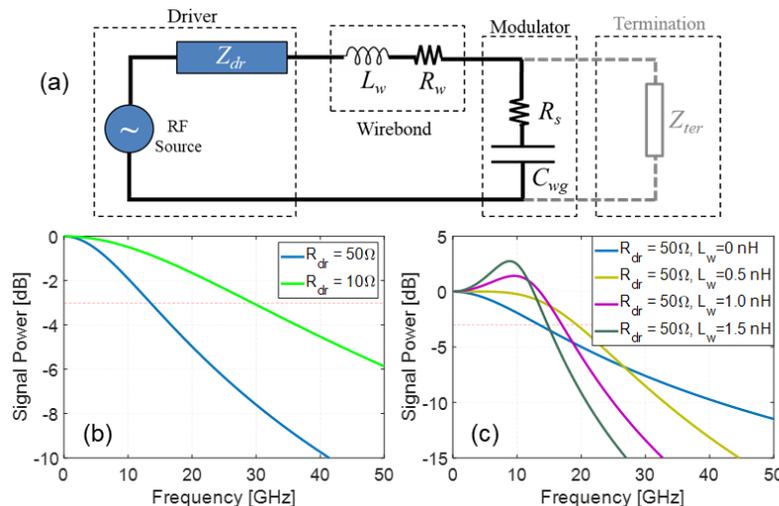

Fig. 1. (a) Equivalent circuit in LE configuration. (b) Signal power delivered to the LE modulator using a 50 Ω (blue) and 10 Ω (green) driver. In (c), an additional inductance arising from wire-bonds is also taken into account. The blue curve serves as reference and is identical to the blue curve in (b). The driver output impedance is kept at 50 Ω. The termination (grayed out in Fig 1(a)) is usually not used when driving an LE modulator with a close by driver. It is indicated here to support the discussion in Section 3.

While Eq. (3) is well known, it plays a particularly important role in the case of meandered LE modulators, since the capacitance of the device scales with the optical length of the phase shifter, which is no longer constrained to be on the order of, or stay below a fraction of λ_{RF}. Other limitations then come into play in limiting the device length, such as the RC bandwidth limitation as described above. This is quantitatively shown in Fig. 1(b) assuming the device length to be 500 μm and the phase shifter configuration to be W1 (lowest doping) as described in the following (with linear capacitance and resistance of C_l=260 pF/m and R_l=17 mΩ·m). It can be seen that replacing the 50 Ω connection by a low impedance

(10 Ω) driver increases the bandwidth from 14 GHz (blue curve) to 28 GHz (green curve). The signal power (voltage squared) delivered to the device is plotted as calculated based on the lumped equivalent circuit, which is equivalent to the electro-optic S_{21} of the modulator, provided that the actuation speed is the only parameter limiting the device bandwidth.

Apart from the output impedance of the driver, the series inductance induced by wire bonds also plays a role in the frequency response of the device. Together with the phase shifter capacitance, it forms an LC resonator which results in a peaking response in the S_{21} of the modulator. This can potentially increase the device bandwidth provided that the resonance frequency is close to or slightly above the RC cutoff frequency of the device. However, it can also distort the modulated signal if the inductance is so large that the resonance frequency falls substantially below the RC cutoff. To quantify this, we can estimate the inductance of a wire bond with 25 µm of diameter used to connect a driver with the LE modulator, with the rule of thumb of 1 nH/mm [15]. In Fig. 1(c), the blue curve for a 50 Ω driver does not take the wire-bond inductance into account, and is kept as a reference. The other curves correspond respectively to 0.5 mm, 1 mm and 1.5 mm long wire-bonds. A small additional inductance can increase the cutoff frequency to 19 GHz (yellow curve). However, further increase of the series inductance reduces the bandwidth and distorts the signal. Here too, the parasitic inductance associated to the driving scheme limits the maximum optical length of the meandered phase shifter.

Transit time of the light

While the RC bandwidth limitation described above is well known, as second limiting factor that commonly plays much less of a role, but is of primary importance here, is the time taken for light to transit through the device. Indeed, in a conventional rectilinear LE phase shifter the optical length is also on the order of $\lambda_{RF}/10$, since the optical length coincides with the RF length. In a meandered device, the optical phase shifter length is however much longer and is ultimately limited by the photon transit time if a specific electro-optic cutoff frequency is to be maintained, similarly to what happens in an RRM in regards to the maximum allowable storage time [9].

In a LE device, it can be assumed that the same voltage is applied along the entire device length. It can thus be simply written as $V = V_0 cos(\omega_{RF}t)$, where V_0 is the amplitude of the RF signal and ω_{RF} its angular frequency. The time τ_g taken by photons to pass through the device can be simply calculated as $\tau_g = l/(c_0/n_g)$, with n_g the waveguide's group index. At low frequencies, defined by $\omega_{RF}\tau_g \ll 1$, the maximum (minimum) applied phase shifts simply depend on the applied voltage V_0 and the phase shifting efficiency of the device, and coincides with the DC response of the modulator. At high frequencies, at which τ_g is comparable with the RF period, the maximum (minimum) phase shifts are reached for photons entering the device at the time $t_{in} = -\tau_g/2$ before the RF signal reaches its maximum (minimum) and exiting it at $t_{out} = \tau_g/2$ after the maximum (minimum) of the RF signal. Thus, the frequency dependent phase shift can be written as

$$\frac{\Delta\varphi(\omega_{RF})}{\Delta\varphi(0)} = \frac{1}{\tau_g}\int_{-\tau_g/2}^{\tau_g/2}\cos(\omega_{RF}t)dt \tag{4}$$

The integral corresponds to the efficiency reduction of the phase shifter at ω_{RF} compared to DC, due to the "smearing out" of the drive voltage as averaged over the transit time. The -3dB cutoff is reached when this ratio equals $1/\sqrt{2}$. Hence,

$$\frac{\Delta\varphi(\omega_{RF})}{\Delta\varphi(0)} = \frac{2}{\tau_g}\frac{\sin(\omega_{RF}\tau_g/2)}{\omega_{RF}} = \frac{1}{\sqrt{2}} \tag{5}$$

which yields $\omega_{RF} = 2.79/\tau_g$. Thus, the device's E/O bandwidth can be written as $f_{-3dB,opt} \approx 0.44/\tau_g$.

2.2 Power consumption in LE modulators

As already explained above, it is in general unclear whether LE or TW devices have the lower power consumption: While LE do not have a termination resistor and thus only dissipate power when data levels are switched, rectilinear LE modulators are also in general much shorter and thus require higher drive voltages. When operated with a distributed driver [14], they are no longer limited by phase matching and can be implemented with equally long (or even longer) phase shifters, so that they combine the best of both worlds and can reach much lower power consumption levels. Similarly, within the limits described in Subsection 2.1, meandered phase shifters can be implemented with relatively long optical lengths, so that here too power consumption reduction is expected without the complexity associated to the implementation of distributed drivers.

A detailed comparison between the power consumption of LE and TW modulators can be found in the Appendix of [16], a short summary of which is given here to allow comparing the RF power consumption of the different modulation configurations that are being discussed. Since the analysis in [16] is aimed primarily at LE phase shifters driven by distributed drivers, whose cumulative lengths are not limited by phase matching or the photon transit time, its applicability to M-MZMs has some limitations discussed in the following.

In an unterminated carrier-depletion LE modulator, modulation boils down to charging and discharging a capacitor. The average power consumption per bit has already been given by Eq. (1), wherein the total capacitance C already takes into account that there are two phase shifters in an MZM operated in push-pull configuration. On the other hand, the total power consumption in a TW-MZM can be calculated as [16]

$$P_{TW} = \frac{V_D^2}{Z_{TL}} \tag{6}$$

with Z_{TL} the characteristic impedance of a single MZM arm and V_D the drive voltage. Again, this assumes driving in push-pull configuration. During modulation, V_D is applied across one of the arms, during which time the voltage applied across the other arm is set to zero, and thus does not result in internal power consumption inside the MZM. Moreover, this is only valid when the signal is DC-biased at half of the drive voltage swing. While biasing a carrier-depletion MZM at a higher reverse voltage results in a reduced junction capacitance and thus a higher bandwidth (as done for example in [17]), this can also be achieved by introducing a small intrinsic region inside the junction, so that Eq. (6) remains a representative expression for TW-MZM power consumption.

In order to compare P_{TW} [Eq. (6)] with $E_{bit,LE}$ [Eq. (1)], i.e., to convert P_{TW} into an energy per bit, we need to know the cutoff frequency of the TW-MZM, so as to predict the maximum data rate it can support. Taking into account the screening of the capacitive load at high frequencies approaching the RC cutoff of the phase shifter [16], we can express the RF power loss along the waveguide as

$$\frac{dV}{dx} = -\frac{1}{2} \frac{R_l \cdot Z_{TL}(\omega_{RF} C_l)^2}{1 + (R_l C_l \omega_{RF})} V \tag{7}$$

with V the voltage along the phase shifter, x the propagation direction, and ω_{RF} the angular frequency at which the modulator is operated. At the intrinsic cutoff frequency ($\omega_{RF} = \omega_c$) based on Eq. (2), Eq. (7) reduces to $-1/4(R_l Z_{TL} \omega_c^2 C_l^2)$ [16]. If the bandwidth of the TW modulator were only limited by the RF loss along the waveguide, we could assume the device length to be 74% of the 1/e voltage decay length of the phase shifters (corresponding to an RF loss of -6.4 dB). Sizing the modulator this way however results in an overall cutoff frequency that is a bit below ω_c since screening of the capacitive load results in a second bandwidth limitation, on the order of $\omega_{TW,-3dB} = 0.6/R_l C_l$ [16]. Since for on-off keying the electro-optic cutoff frequency is typically on the order of 70% the data rate D, it can be assumed that $D \approx 0.86/2\pi R_l C_l \approx 0.14 \omega_c$. Based on the previous assumptions, l is given by

$$l = 0.74 \frac{4}{R_l \cdot Z_{TL}(\omega_c C_l)^2} = \frac{2.96}{Z_{TL} \omega_c C_l} \tag{8}$$

Combining Eqs. (1), (6) and (8), and further assuming the data rate of the TW-MZM to be $0.14 \omega_c$, we obtain

$$E_{bit,TW} = 5 \cdot E_{bit,LE} \tag{9}$$

assuming the TW- and the LE-MZMs to have the same phase shifter length and to be driven with the same maximum drive voltage. By changing the driving scheme from TW to LE for the same phase shifter, the power consumption is thus reduced by a factor in the order of 5.

In the above, we made an assumption on the TW-MZM phase shifter length: We assumed the TW-MZM was sized so that RF losses along the transmission line and the intrinsic cutoff frequency of the diode equally contribute to the overall cutoff frequency of the modulator. While this is a sensible assumption to make in many cases [16], it is not generally true. However, if we take as a figure of merit the maximum supported data rate divided by the energy per bit, we find that the LE-enhancement is above ~6 irrespectively of how we size the (equal) lengths of the modulators [16]. Since this figure of merit empirically also appears to be a good predictor for the performance tradeoffs that can be made in carrier-depletion phase shifter configurations (i.e., redesign of the phase shifter cross-section) [9,16], this enhancement appears to be a good rule of thumb even when the freedom is given to redesign the phase shifter geometry. The second assumption is for the

LE-MZM to have the same phase shifter length. In case of the M-MZM described in the following, this level of enhancement can thus only be expected if its cutoff frequency is limited by its intrinsic RC time-constant. If, on the other hand, the photon transit time is the limiting factor and the M-MZM length limited by it, the improvement will be less, so that it has to be looked at carefully in the following.

3. LUMPED ELEMENT MEANDERED MODULATOR

To shrink the size of the modulator below the lumped element condition while simultaneously keeping the phase shifter length suitable for low drive voltage operation, we propose the meandered modulator configuration as shown in Fig. 2(b). First, we describe the device design, its simulated performance, and its layout. Next, we report the measurement results obtained from the fabricated devices and discuss potential improvements.

3.1 Concept and design

A short modulator with a length of 250 µm can be regarded as a lumped element device (based on the LE condition $l_{RF} < \lambda_{RF}/10$) up to 30 GHz assuming n_{RF} to be ~4. Assuming the modulation efficiency $V_\pi l$ of a conventional, rectilinear LE phase shifter [Fig. 2(a)] to be 2 V·cm (as is the case for typical depletion based modulators such as reported in [18]), the drive voltage required for each arm of the MZM to reach a π/2 phase shift (for full extinction) is as high as 40 V. Since the drive voltage generated by high-speed CMOS electronics is limited to about 2 V_{pp}, this severely penalizes the extinction ratio (ER) and resulting eye opening. To increase the achievable phase shift, we meander the phase shifter as shown in Fig. 2(b). In this device, the RF length of the modulator, i.e., the length of the electrodes, is still kept at 250 µm, but the optical phase shifter length of the device is 1.4 mm. This reduces the required drive voltage from 40 V_{pp} to 7 V_{pp} for the same phase shifter technology (same cross-section). The benefits associated to the LE configuration, as discussed in Section 2, are still applicable to this structure, provided that the device remains unterminated.
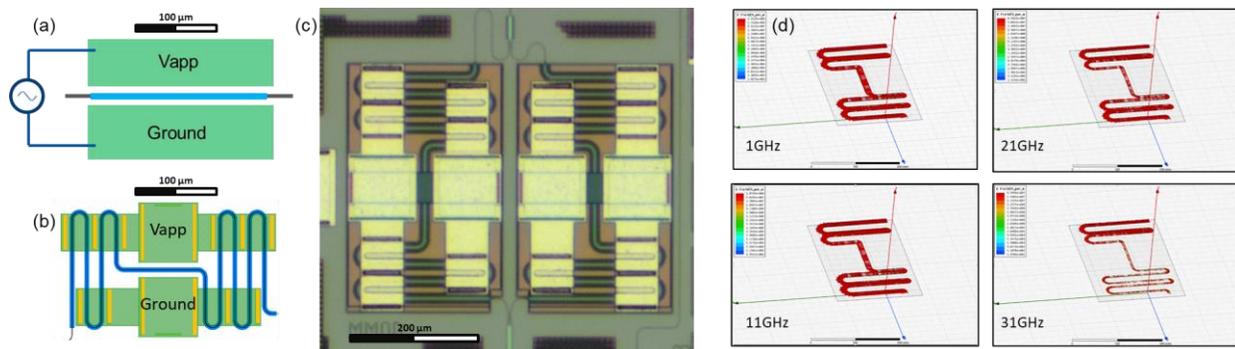

Fig. 2. (a) Schematic of a conventional, rectilinear LE device. (b) Actual layout of one arm of the meandered modulator. The yellow strips show the vias, connecting the top metal layer to the device. (c) Microscope image of the fabricated meandered MZM. (d) 3D HFSS simulation of the device, at 4 different frequencies and maximum applied voltage. Red arrows show the field strength.

Fig. 2(c) shows a micrograph of the fabricated device. It was fabricated in the standard silicon photonics process of Singapore's Institute of Microelectronics (IME/A*STAR) in silicon-on-insulator (SOI) wafers with a 220 nm thick silicon device layer, with process splits applied to the diode doping concentrations. We used one-by-two multi-mode interferometers (MMIs) both at the input and output of the MZM, which was also slightly imbalanced to facilitate phase shift measurements. Vias are placed in the vicinity of the waveguides to minimize current flow through the silicon [Fig. 2(b)]. They drop onto highly doped silicon starting 600 nm from the edge of the waveguide, as a tradeoff between waveguide losses and series resistance. Thanks to the high index contrast between silicon and oxide which allows for small bending radii, geometrical constraints on how much waveguide length can be fit into a small area is not an essential limiting factor here. Rather, the photon transit time (as explained in Subsection 2.1) emerges as a main limitation trading off device bandwidth with drive voltage. Based on Eq. (5), $f_{-3dB,opt}$ is about 25 GHz for our 1.4 mm long phase shifter, given that the group index of the 400 nm wide, 120 nm etched waveguide is calculated to be 3.8. The second factor limiting the device length is of course the insertion loss. The meandered modulators were fabricated on three different wafers with identical layout and fabrication process apart from the phase shifter doping as summarized in Table 1. The three wafers W1-W3 are subjected to increasingly strong doping in the waveguides, so that expected optical insertion losses and drive voltages for full extinction also vary as 2.3 dB, 4.7 dB, 8.6 dB and 8.6 V_{pp}, 4.7 V_{pp}, and 3.7 V_{pp}, respectively. In addition

to doping induced losses (6 dB/cm, 23 dB/cm and 51 dB/cm), 3 dB/cm roughness and surface passivation induced waveguide losses as well as 0.5 dB per MMI are also factored in.

Based on the length of the device, taking the maximum metal distance as the device RF length, the device is expected to behave as an LE (same voltage along the device) at least up to 25 GHz. However, in order to accurately determine the voltage received by each point along the phase shifter, a 3D simulation is required as a verification. From this data and from the group index n_g of the optical mode, one can calculate the exact frequency dependent OMA penalty for high frequencies beyond the LE condition, according to [9]

$$\frac{\Delta\varphi(\omega_{RF})}{\Delta\varphi(0)} = \frac{1}{V_0 l}\int_0^l |V(z)|e^{i\omega_{RF}\left(\frac{z\cdot n_g}{c_0}\right)+i\varphi_{RF}(z)}\,dz \tag{10}$$

where z is the curvilinear coordinate along the phase shifter, and $|V(z)|$ and φ_{RF} are respectively the magnitude and phase of the applied RF voltage. For this purpose, the layout of the device is exported to an RF field simulator (HFSS) and the field along the waveguide calculated, as shown in Fig. 2(d). The simulations confirm that below 25 GHz the field applied across the phase shifter has no position (z-)dependent phase delay and the device can thus be regarded as an LE. Since the device bandwidth is limited to 25 GHz due to a combination of photon transit time and electric time constant, the electro-optic cutoff frequency of the device is calculated with the assumption of LE behavior, simply using the equivalent circuit shown in Fig. 1(a) in combination with the photon transit time limitation.
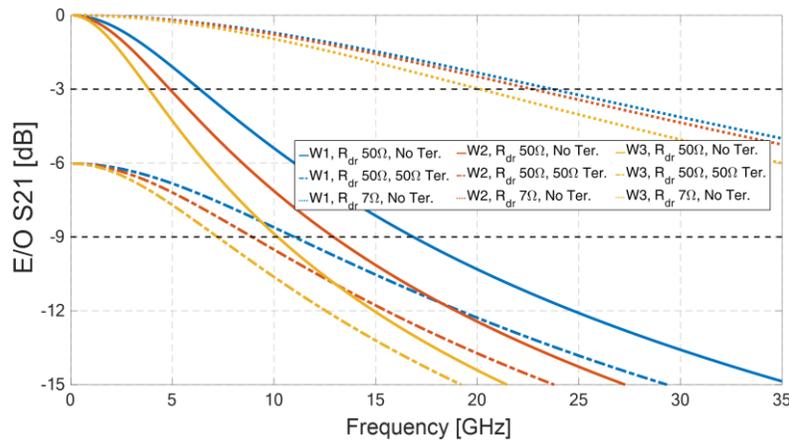

Fig. 3. Simulated electro-optic response (S₂₁) of the low doped (blue, W1), medium doped (red, W2) and highly doped (yellow, W3) LE meandered modulators. Solid lines: 50 Ω driver output impedance and device not terminated. Dashed lines: 50 Ω driver output impedance and device 50 Ω terminated. Dotted lines: 7 Ω driver output impedance without termination. The model only takes the lumped element circuit shown in Fig. 1(a) into account, photon transit time is accounted for separately.

The RC limited bandwidth $f_{-3dB,RC}$ also depends on the driver output impedance. Fig. 3 shows the electro-optic S₂₁ of the device, assuming that it is only limited by the voltage delivered to the capacitive load based on the equivalent lumped element circuit [Fig. 1(a)]; the photon transit time is accounted for separately in the following. The solid lines show the case of the device being driven using 50 Ω probes and not being terminated. It predicts the electrical cutoff frequency $f_{-3dB,RC}$ of the devices to be 6.3 GHz, 4.8 GHz, and 3.9 GHz for W1, W2 and W3, respectively. The dotted lines show the device bandwidth when driven by a 7 Ω driver, also without termination. In this case, the cutoff frequencies of W1, W2 and W3 are calculated to be 23.7 GHz, 22.7 GHz, and 20.1 GHz, respectively. In the fabricated chips, that were meant to be characterized in a 50 Ω environment, we terminated the LE modulators with a 50 Ω on-chip resistor [greyed out in Fig. 1(a)]. In principle, this goes against the purpose of the LE modulators, but allowed higher speed measurements in a 50 Ω environment and validation of the models in the absence of co-packaged low output impedance drivers. The predicted electro-optic response of the device in this configuration is plotted in Fig. 3 with dashed lines. It predicts the cutoff frequencies for W1, W2, and W3 to be 11 GHz, 8.9 GHz, and 7.3 GHz, respectively. This can be achieved at the expense of 6 dB reduction in OMA at low frequencies compared to an unterminated device in an ideal 50 Ω environment in which the induced back-reflection is fully absorbed by the driver (with the voltage at the device doubling due to the capacitive termination, respectively the 50 Ω termination forming a voltage divider with the output impedance of the driver in the 50 Ω terminated case).

The photon transit time also reduces the bandwidth. The overall bandwidth of the device can be estimated as

$$f_{-3dB} = \left(\frac{1}{f_{-3dB,RC}^2} + \frac{1}{f_{-3dB,opt}^2} \right)^{-1/2}$$

(11)

The overall bandwidth of the devices for the three configurations discussed above and for the three different doping levels are summarized in Table 1. With the 50 Ω on-chip termination driven by 50 Ω cables, as is the case for the characterization reported in the next subsection, the cutoff frequencies of W1, W2 and W3 are expected to be 10.1 GHz, 8.3 GHz, and 7 GHz.

Table 1. Simulated performance of the meandered modulators

Doping level		Ph. Shift. length	Δn_{eff} at -2V	E/O f_{-3dB} @ -2 V bias		
				No termination		50 Ω ter.
P-doping	N-doping			R_{dr}=50 Ω	R_{dr}=7 Ω	R_{dr}=50 Ω
W1	1.3e17 cm⁻³	4e17 cm⁻³	1.4 mm	6e-5	6.1 GHz	17.1 GHz	10.1 GHz
W2	9e17 cm⁻³	1.1e18 cm⁻³	1.4 mm	11e-5	4.7 GHz	16.8 GHz	8.3 GHz
W3	2.1e18 cm⁻³	2.6e18 cm⁻³	1.4 mm	14e-5	3.9 GHz	15.6 GHz	7.0 GHz

3.2 Experimental results and discussion

A micrograph of a fabricated M-MZM is shown in Fig. 2(c). As mentioned, the devices are fabricated on three different wafers, W1, W2, and W3, with different doping levels. Using a tunable laser (1.49 μm to 1.61 μm), we measure the optical transmission of the devices. After de-embedding the optical loss of the grating couplers (~9 dB for a grating coupler pair), the insertion loss of the three devices are measured to be 5 dB, 6.3 dB, and 9.1 dB for W1, W2, and W3, respectively. The dependence on doping concentration is only 65% of the simulated dependence, which could point to overall lower dopant levels inside the waveguides. However, there appears to be an additional fixed ~3 dB losses added to all of the devices. The bending loss of the meandered modulators was assumed to be negligible, which could be one source of discrepancy, in particular if the etch depth turned out to be less than nominal, in which case dopants in the contact regions could also play more of a role. The lower metal layer also has several crossings with the waveguides, which we have observed to lead to excess losses in other structures on the chip.
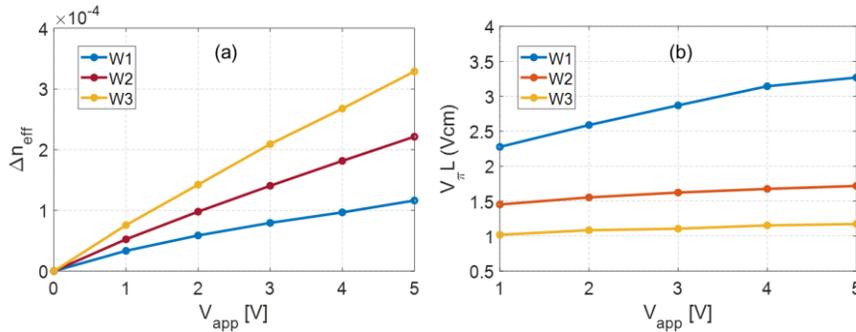

Fig. 4. Measured effective index change (a) and phase shift efficiency $V_\pi l$ in V·cm (b) versus the applied reverse bias voltage for the three doping levels.

The measured $V_\pi l$ and the extracted effective index change are shown in Fig. 4 as a function of applied voltages. Since the meandered modulators themselves are in parallel with a 50 Ω termination resistor, these measurements were performed on linear 1 mm and 2 mm long phase shifters, which have the exact same phase shifter cross-section, but are unterminated and can thus be measured with high DC voltages without thermal runoff. The measurement results are in a good agreement with simulations (cf. Table 1), as effective index changes of 6e-5, 10e-5, and 15e-5 are measured after applying a 2 V reverse bias voltage. The required dual drive voltages to achieve full extinction for W1, W2 and W3 are ~9.2 V$_{pp}$, ~5.5 V$_{pp}$, and ~3.7 V$_{pp}$, respectively, with corresponding $V_\pi l$ of 2.58 V·cm, 1.55 V·cm, and 1.03 V·cm measured at 2 V reverse bias [Fig. 4(b)]. The figure of merit $V_\pi l \cdot \alpha_{dB}$, the product of $V_\pi l$ with the waveguide losses α_{dB}, with overall unit of V·dB, is useful to compare the performance of the three phase shifters. It corresponds to the required drive voltage for a phase

shifter short enough to exhibit 1 dB loss and is calculated as 92 V·dB, 70 V·dB, and 67 V·dB, respectively for W1, W2, and W3. Alternatively, one may use $C_l(V_\pi l)^2/8 \cdot \alpha_{dB}$ in units of dB·pJ/b, which corresponds to the energy per bit for a LE-MZM with phase shifters also sized to have 1 dB of optical losses [9,16]. It is calculated as 77.3 dB·pJ/b, 52.7 dB·pJ/b and 46.6 dB·pJ/b for W1, W2, and W3, respectively. The simulated values for the junction capacitance were used here. These are 2.6 pF/cm, 3.9 pF/cm, and 5.4 pF/cm and are in a good agreement with measurements.

The measured normalized electro-optic S_{21} of the three meandered modulators are plotted in Fig. 5 for different bias voltages. Since all the modulators have an on-chip 50 Ω termination resistor and the RF signal is transmitted to the devices using 50 Ω cables, the cutoff frequencies extracted from these curves should be compared with the last column of Table 1 (the dashed lines in Fig. 3 only take the RC limitation into account). The measured S_{21} curves at -2 V bias cross the -3dB point at 8.7 GHz, 8.1 GHz, and 7 GHz for W1, W2, and W3, respectively, which is in a good agreement with the simulated electro-optic bandwidths.
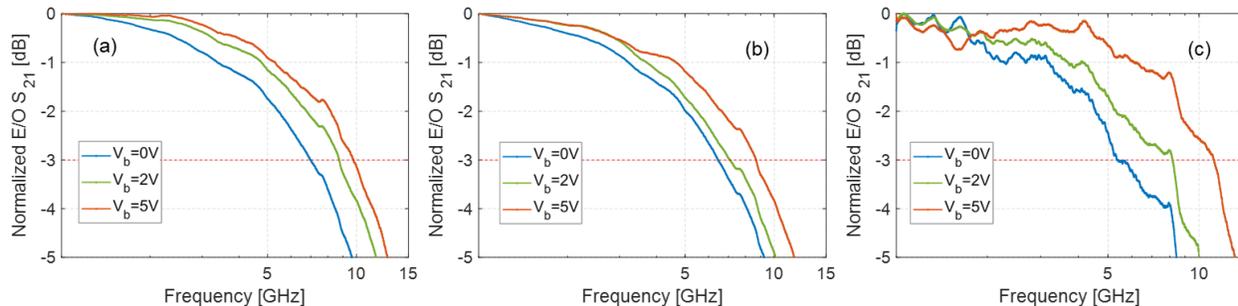

Fig. 5. Measured small-signal electro-optic S_{21} for (a) W1, (b) W2, and (c) W3, using a 50 Ω driver and with 50 Ω on-chip termination.

In order to verify the measured cutoff frequencies of the meandered modulators, we have also performed data transmission tests. The measured eye diagrams for the 3 wafers at different data rates are shown in Fig. 6. For all measurements, the laser power was set to 20 mW, mainly in order to compensate for the 9 dB loss arising from the grating coupler pair, and a 2 V_{pp} signal was applied to the modulators at -2 V bias. These measurements further confirm that the W3 modulator has a smaller bandwidth, as seen in the substantial eye closure at 25 Gb/s. However, devices W1 and W2 feature open eye diagrams up to at 25 Gb/s.
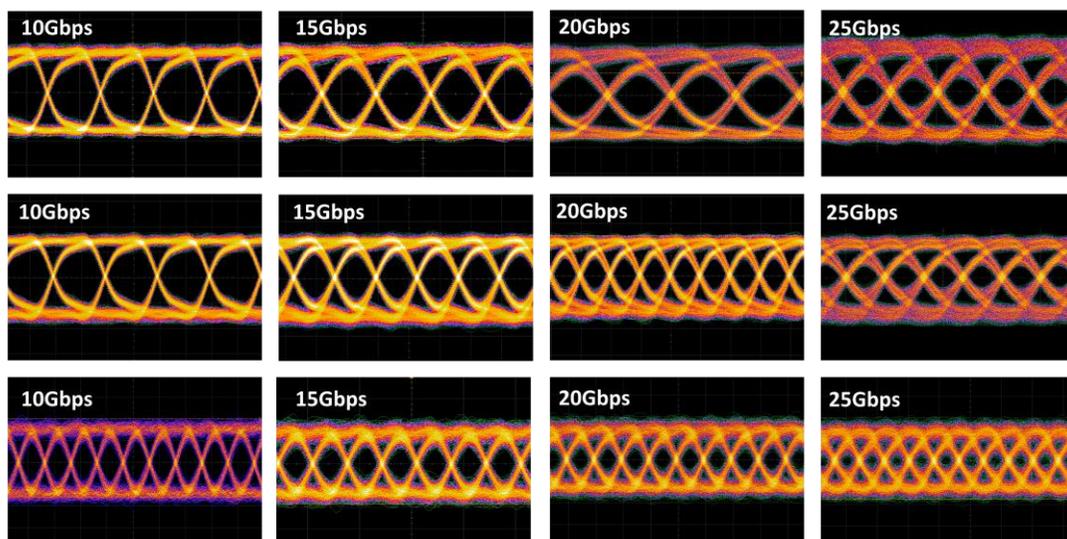

Fig. 6. Measured PRBS15 eye diagrams obtained with a 2 V_{pp} signal with -2 V bias, for W1 (first row), W2 (second row), and W3 (third row) at different data rates recorded by a 20 GHz real-time oscilloscope.

The high frequency performance of the M-MZMs could be substantially improved by wire-bonding a low impedance driver, as a 4Ω output driver [19] would result in a threefold improvement of the RC time constant limited electro-optic bandwidth, so that an overall cutoff frequency of ~18 GHz could be reached (including photon transit time). In order to

further reduce the power consumption of the meandered phase shifter and reduce the requirements on driver output impedance, it would be preferable to replace the Mach-Zehnder interferometer with a Michelson type interferometer [20], which would result in half the capacitance while maintaining the same optical modulation amplitude, photon transit time and insertion loss. As a drawback, such device requires an isolator between laser and modulator to filter out back-reflections.

At this point, we can compare the power consumption of the implemented M-MZMs (explained in details in Section 3) with the power consumption of a TW-MZM implemented with the same phase shifter cross-section as W1 [21]. This TW-MZM has a length of 4 mm, an electro-optic cutoff frequency of 17 GHz, 8.8 dB insertion losses, and a characteristic impedance of 50 Ω. Assuming the maximum available drive voltage, as limited by the chosen integrated circuit (IC) technology, to be 2 V_{pp}, the optimum device length yielding the highest OMA would be on the order of 2.05 mm. Excluding excess losses due to splitters and metal crossings (i.e., assuming the modeled waveguide losses), the modulation and insertion loss penalty (reduction of OMA relative to the power entering the modulator) would be on the order of -7.2 dB and only 0.3 dB better than that of the M-MZM calculated with the same assumptions. Due to the shortening of the phase shifters, the TW-MZM's cutoff frequency would be expected to increase to 21 GHz, also close to the bandwidth expected from the M-MZM when driven with low output impedance drivers. In other words, the TW-MZM would only be marginally better in terms of OMA and bandwidth.

Based on Eq. (6), the RF power consumption of the TW-MZM when driven by a 2 V_{pp} signal is 80 mW (both MZM arms are designed to have a 50 Ω characteristic impedance). On the other hand, for the 1.4 mm long non-terminated M-MZM from W1, based on Eq. (1), the RF power consumption is 20 mW at 28 Gb/s, the typical data rate at which both MZMs would operate (with the data rate ~70% of the cutoff frequency). The M-MZM thus improves the power consumption by a factor ~4 relative to the TW-MZM. As already mentioned above, an additional factor 2 could be reached by using the Michelson interferometer configuration without incurring additional penalties.

4. CONCLUSION

In summary, we introduced meandered MZMs as a new configuration allowing to drive a modulator as a lumped element while keeping the optical length of the phase shifter sufficiently long to achieve an acceptable modulation depth with a 2 V_{pp} drive voltage. Contrary to distributed drivers, it allows driver integration with simple wire bonds. We implemented three devices with different doping levels to test the performance of such devices. The W2 meandered modulator with a moderate doping level of ~1e18 cm^{-3} features a moderate drive voltage of 5.5 V_{pp} (for full extinction) and an insertion loss of 6.3 dB. It features open eye diagrams at 25 Gb/s in a 50 Ω test environment, as enabled by an on-chip termination. The -3dB bandwidth of an unterminated device can be drastically improved, provided that it is wire bonded to a low output impedance driver. We also compared the power consumption of unterminated M-MZMs with a TW-MZM with the same type of phase shifter and showed that the M-MZM results in similar bandwidth and optical modulation amplitude while potentially improving the power consumption by a factor ~4. In Michelson configuration, an additional factor 2 in power consumption reduction could be obtained. Moreover, in contrast to RRMs, the meandered modulators do not impose additional constraints to the control system compared to TW-MZMs, which further helps maintaining a low power consumption and stable uncooled operation. Thus, the M-MZM configuration offers a compact and robust modulation scheme with reduced power consumption at 25 Gb/s.

ACKNOWLEDGEMENTS

REFERENCES

[1] M. He, M. Xu et al., "High-performance hybrid silicon and lithium niobate Mach–Zehnder modulators for 100 Gbit s^{-1} and beyond," Nat. Photonics 13, 359–364 (2019).

[2] M. Li, L. Wang, X. Li, X. Xiao, S. Yu, "Silicon intensity Mach–Zehnder modulator for single lane 100 Gb/s applications," Photon. Res. 6, 109-116 (2018).

[3] S. Zhalehpour, J. Lin, M. Guo, H. Sepehrian et al., "All-Silicon IQ Modulator for 100 GBaud 32QAM Transmissions," in Proc. Optical Fiber Communication Conference (OFC), Th4A.5 (2019).

[4] S. Wolf, H. Zwickel, W. Hartmann et al. "Silicon-Organic Hybrid (SOH) Mach-Zehnder Modulators for 100 Gbit/s on-off Keying," Sci. Rep. 8, 2598 (2018).

[5] A. Narasimha et al., "An ultra-low power CMOS photonics technology platform for H/S optoelectronic transceivers at less than \$1 per Gbps," in Proc. Optical Fiber Communication Conference (OFC), OMV4 (2010).

[6] "Cisco Visual Networking Index: Forecast and Trends, 2017–2022 White Paper, Document ID:1551296909190103," Cisco, February 2019.

[7] S. Sharif Azadeh, F. Merget, M. P. Nezhad, J. Witzens, "On the measurement of the Pockels effect in strained silicon," Opt. Lett. 40(8), 1877–1880 (2015).

[8] G. T. Reed et al., "Recent breakthroughs in carrier depletion based silicon optical modulators," Nanophotonics 3(4-5), 229-245 (2014).

[9] J. Witzens, "High-Speed Silicon Photonics Modulators," Proceedings of the IEEE 106(12), 2158-2182 (2018).

[10] S. Romero-García et al., "Broadband, temperature tolerant and passively biased resonantly enhanced Mach-Zehnder modulators," in Proc. 13th IEEE Conference on Nano/Micro Engineered and Molecular Systems (NEMS), 668-674 (2018).

[11] H. Nguyen, S. Hashimoto, M. Shinkawa, T. Baba, "Compact and fast photonic crystal silicon optical modulators," Opt. Express 20(1), 22465-22474 (2013).

[12] S. Romero-García, A. Moscoso-Mártir, S. S. Azadeh, J. Müller, B. Shen, F. Merget, J. Witzens, "High-speed resonantly enhanced silicon photonics modulator with a large operating temperature range," Opt. Express 42(1), 81-84, (2017).

[13] D. Miller, "Energy consumption in optical modulators for interconnects," Opt. Express 21(S2), A293-A308 (2012).

[14] D. Kucharski et al., "Distributed amplifier optical modulator," US Patent 7,899,276 (2011).

[15] D. Michelon, E. Bergeret, M. Egels, A. D. Giacomo, "Wire-bonds used as matching inductor in RF energy harvesting applications," in Proc. 10th Conference on Ph.D. Research in Microelectronics and Electronics (PRIME), 1-4 (2014).

[16] S. S. Azadeh et al., "Low $V\pi$ Silicon photonics modulators with highly linear epitaxially grown phase shifters," Opt. Express 23(18), 23526-23550 (2015).

[17] P. Dong, L. Chen, Y.-K. Chen, "High-speed low-voltage single-drive push-pull silicon Mach-Zehnder modulators," Opt. Express 20(6), 6163-6169 (2012).

[18] S. Sharif Azadeh, J. Müller, F. Merget, S. Romero-García, B. Shen, J. Witzens, "Advances in silicon photonics segmented electrode Mach-Zehnder modulators and peaking enhanced resonant devices," in Proc. SPIE 9288, 928817 (2014).

[19] A. Moscoso-Mártir et al., "Silicon Photonics Transmitter with SOA and Semiconductor Mode-Locked Laser," Sci. Rep. 7, 13857 (2017).

[20] X. Li et al., "Highly efficient silicon Michelson interferometer modulators," IEEE Photon. Technol. Lett. 25(5), 407-409 (2013).

[21] F. Merget, S. Sharif Azadeh, J. Müller, B. Shen, M. P. Nezhad, J. Hauck, J. Witzens, "Silicon photonics plasma modulators with advanced transmission line design," Opt. Express 21(17), 19593-19607 (2013).